Title

Improved force-field parameters for QM/MM simulations of the energies of adsorption for molecules in zeolites and a free rotor correction to the rigid rotor harmonic oscillator model for adsorption enthalpies

Journal

Journal of Physical Chemistry C, 119(4)

ISSN

1932-7447

Authors

Li, YP
Gomes, J
Sharada, SM
et al.

Publication Date

2015-01-29

DOI

10.1021/jp509921r

Peer reviewed

THE JOURNAL OF PHYSICAL CHEMISTRY C

Article

pubs.acs.org/JPCC

Improved Force-Field Parameters for QM/MM Simulations of the Energies of Adsorption for Molecules in Zeolites and a Free Rotor Correction to the Rigid Rotor Harmonic Oscillator Model for Adsorption Enthalpies

Yi-Pei Li,[†] Joseph Gomes,[†] Shaama Mallikarjun Sharada,[†] Alexis T. Bell,[†] and Martin Head-Gordon*[,‡]

[†]Department of Chemical and Biomolecular Engineering and [‡]Department of Chemistry, University of California, Berkeley, California 94720-1462, United States

ABSTRACT: Quantum mechanics/molecular mechanics (QM/MM) simulations provide an efficient avenue for studying reactions catalyzed in zeolite systems; however, the accuracy of such calculations is highly dependent on the zeolite MM parameters used. Previously reported parameters (P1), which were chosen to minimize the root mean square (RMS) deviations of adsorption energies compared with full QM ωB97X-D/6-31+G** adsorption energies, are shown to overestimate binding energies compared with experimental values, particularly for larger substrates. To address this issue, a new parameter set (P2) is derived by rescaling the previously reported characteristic energies of the Lennard-Jones potential in P1. The accuracy of the thermal correction for adsorption enthalpies determined by the rigid rotor-harmonic oscillator approximation (RRHO) is examined and shown to be improved by treating low-lying vibrational modes as free translational and rotational modes via a quasi-RRHO model. With P2 and quasi-RRHO, adsorption energies calculated with QM/MM agree with experimental values with an RMS error of 1.8 kcal/mol for both nonpolar and polar molecules adsorbed in MFI, H-MFI, and H-BEA. By contrast, the RMS error for the same test sets obtained using parameter set P1 is 8.3 kcal/mol. Glucose−fructose isomerization catalyzed by Sn-BEA is taken as an example to demonstrate that improved values for apparent activation energies can be obtained using the methodology reported here. With parameter set P2, the apparent activation energy calculated with QM/MM reproduces the experimental value to within 1 kcal/mol. By contrast, using parameter set P1, the error is −12.9 kcal/mol.

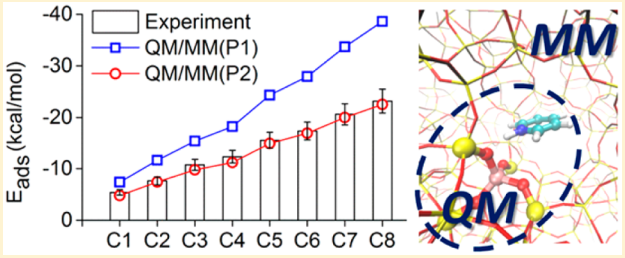

INTRODUCTION

Zeolites in their Brønsted or Lewis acid form are active catalysts for a variety of chemical reactions involved in the production of transportation fuels and special chemicals, e.g., hydrocarbon cracking, isomerization, and alkylation.[1−3] Experimental studies have shown that the catalytic activity and product selectivity for such reactions are highly affected by the zeolite framework structure and composition, e.g., Si/Al ratio.[4,5] Since the range of possible zeolite structures and compositions is extremely large, it is highly desirable to predict the effects of zeolite frameworks and compositions on catalyst activity and selectivity for a given reaction. Significant progress toward this end has been achieved using quantum chemical simulations based on density functional theory (DFT).[6] Such calculations can not only confirm the interpretations of reaction mechanisms deduced from experimental results but also predict the influence of zeolite framework structure and composition on a reaction.

However, special care has to be taken in order to calculate the interaction between a reactant and a zeolite cluster correctly because long-range dispersion forces are notoriously difficult to handle in ab initio calculations.[7] Recent studies recommend that, for large molecular complexes, dispersion-corrected DFT with valence triple-ζ basis sets should be used.[8] Additionally, an explicit correction should be made for the nonadditive Axilrod−Teller−Muto three-body dispersion interaction, which increases with system size, in order to obtain accurate dispersion interaction energies.[8] However, at this level of theory, it is not feasible to include a significant part of the zeolite framework into the model because of the high computational costs. On the other hand, a zeolite model with only a small cluster (less than 150 tetrahedral atoms; <T150) cannot fully describe the confinement and dispersion effects occurring in the pores of a zeolite.[9]

The recent development of quantum mechanics/molecular mechanics (QM/MM) models offers the possibility of striking a balance between simulation realism, accuracy, and computational costs.[10−14] In QM/MM, a small cluster encompassing the active center and the adsorbate is described by QM, while the rest of the zeolite is described by MM. Zimmerman et al. have selected and validated MM parameters (P1) for

Received: October 1, 2014
Revised: December 18, 2014
Published: December 23, 2014

DOI: 10.1021/jp509921r
J. Phys. Chem. C 2015, 119, 1840−1850

electrostatically embedded QM/MM zeolite simulations by reducing the root mean square (RMS) deviation between QM/MM and QM calculations over a range of adsorption energies and transition states in MFI and H-MFI.[15] Those calculations were done with clusters no larger than 44 tetrahedral atoms in which a T5 QM region is treated at the ωB97X-D[16,17]/6-31+G** level of theory. It was shown that QM/MM(P1) can accurately reproduce QM geometries and QM energetics calculated with the same level of theory and cluster sizes to within ∼2 kcal/mol. Gomes et al. have further validated the scheme with the same parameters by comparing experimental adsorption and activation energies with the values calculated using much larger clusters (>T150) with larger basis sets (ωB97X-D/6-311++G(3df,3pd)) for the T5 QM region.[9] It was shown that the adsorption energy of methanol and the reaction barrier for the methylation of ethene in H-MFI were in good agreement with experimental values, while the adsorption energy of 1-butene in both MFI and H-MFI was overestimated by ∼10%. This overbinding is even more pronounced for larger adsorbate molecules (pentane and hexane), as shown by the recent work of Sharada et al.[18]

Here, we show that the deviation between experimentally measured heats of adsorption for C_1 to C_8 *n*-alkane in siliceous MFI and those calculated with QM/MM(P1) diverges with increasing number of CH_2 units in the adsorbate. We believe that this deviation is due to overestimation of the van der Waals interaction between adsorbates and adsorbents, which constitutes the predominant interaction between alkanes and siliceous zeolites.[15] Since this interaction is modeled by the pairwise-additive Lennard-Jones potential in the QM/MM scheme, it is not surprising to see the error accumulating as the number of significantly interacting pairs of atoms between a guest molecule and a zeolite cluster increases. Since a previous study has shown that intrinsic activation energies calculated using the QM/MM approach, which are most sensitive to MM charge parameters, agree well with experimental values, we believe the MM charges assigned to Si and O of zeolite clusters are reasonable.[18]

The first purpose of this paper is to describe the development and testing of a new parameter set (P2) for describing the adsorption of both nonpolar and polar adsorbates. The P2 parameter set is derived by recalibrating the characteristic energies of the Lennard-Jones potential for O and Si (ε_O and ε_{Si}) in P1 but keeping the MM charge parameters unchanged. With QM/MM(P2), the experimental interaction energies for both physisorption and chemisorption of guest molecules of varying sizes in MFI and H-MFI can be reproduced with errors roughly 5 times smaller than QM/MM(P1). The transferability of the P2 parameters to other zeolites was validated by successful reproduction of the adsorption energies for H-BEA zeolites.

The second goal of this paper is to demonstrate that improved values for the adsorption enthalpies of molecules in zeolites can be obtained by correcting the usual rigid rotor harmonic oscillator (RRHO) model that is used to evaluate zero-point energy and thermal corrections to adsorption enthalpies. By investigating the lower and upper limits to the corrections corresponding to mobile and immobile adsorption, we show that the usual RRHO model is outside the resulting physically allowed regime as temperature rises above room temperature. We show that more physical behavior can be obtained by interpolating between the RRHO model and free rotor contributions as a function of vibrational frequency. The resulting quasi-RRHO model yields improved adsorption enthalpies.

Glucose to fructose isomerization in Sn-BEA is taken as an example to illustrate the application of the new parameter set P2 and the quasi-RRHO model. At the end of the present work, the question of how to simulate reactions occurring in zeolites efficiently and accurately with the QM/MM model is discussed in detail.

METHODS

Zeolite Model Geometries. The crystallographic structures of MFI and BEA were used to determine the positions of all atoms in the zeolite cluster models.[19−21] As shown in Figure 1, a T437 cluster and a T208 cluster were chosen to represent MFI and BEA, respectively. Each cluster was terminated with hydrogen atoms by replacing the terminal oxygen atoms. The H form of the zeolites (H-MFI, H-BEA) was produced by replacing a Si atom in the framework by an Al atom and also introducing a proton to compensate the resulting charge

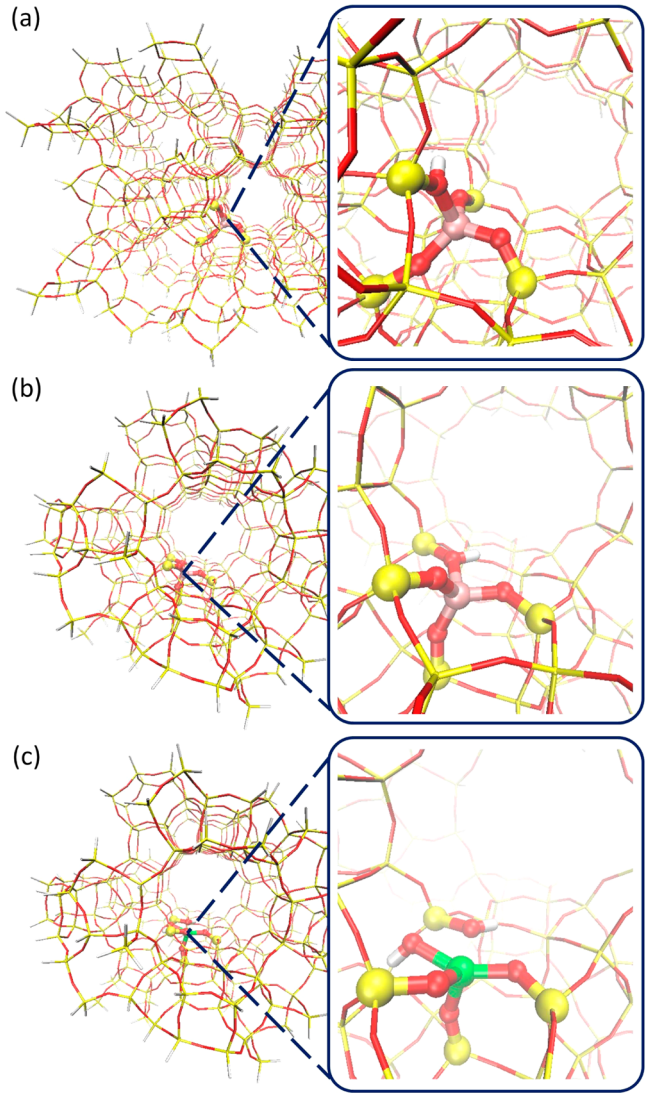

Figure 1. QM/MM models for (a) H-MFI (T437), (b) H-BEA (T208), and (c) Sn-BEA (T208). Atoms shown in yellow, red, pink, white, and green represent Si, O, Al, H, and Sn atoms, respectively. Spherical atoms are QM atoms, others are MM atoms.

DOI: 10.1021/jp509921r
J. Phys. Chem. C 2015, 119, 1840−1850

imbalance. Although the MFI unit cell has 12 different crystallographic sites in which an Al atom can be substituted, there is evidence that the T12 site is favored.[22,23] BEA has nine unique T atom positions, of which two sites were suggested to be most energetically favored for Al atom substitution,[24] i.e., the T1 and T2 sites in the nomenclature of Newsam et al.[20] For this study, we considered the Al atom to be in the T12 site of MFI and the T2 site of BEA. Sn-BEA was produced by replacing a Si atom by a Sn atom in the T2 site, one of the two sites favored for Sn substitution.[25,26] One of the Sn−O−Si bridges was replaced by Sn−OH and Si−OH because previous studies have suggested that this partially hydrolyzed open site is more active than the fully coordinated closed site.[27−29] More discussions of the activity difference between the open and closed sites can be found in our recent work.[30]

Computations. Implementation of the electrostatically embedded QM/MM zeolite model in this work followed the scheme proposed previously, the details of which can be found elsewhere.[15] Adsorbates and a T5 cluster encompassing the active center were described by QM, while the rest of the zeolite was described by MM with a standard force field of the CHARMM type.[31−33] All the geometry optimizations were performed with relaxation of only the internal QM region, keeping all the MM atoms frozen. The hydrogen terminations of the QM region were kept along each of the terminal Si−O bonds at a distance of 0.92 R(Si−O) from the terminal Si atom. Since the MM atoms are held fixed, the only relevant terms in the force field are the two MM−QM interactions. The electrostatic part of this interaction is described by

$$V_{\mathrm{QM/MM}} = \sum_{ij} \frac{q_j}{4\pi\varepsilon_0 r_{ij}} \tag{1}$$

where $V_{\mathrm{QM/MM}}$ is the electric potential in the QM Hamiltonian due to all the MM atoms; r_{ij} is the distance between particles i and j, where particle i is in the QM region and particle j is in the MM region; q_j is the charges on particles j, which is a force-field parameter; and ε_0 is the permittivity of free space. The Lennard-Jones interaction E_{LJ} is given by

$$E_{\mathrm{LJ}} = \sum_{ij} \varepsilon_{ij}\left[\left(\frac{R_{ij}}{r_{ij}}\right)^{12} - 2\left(\frac{R_{ij}}{r_{ij}}\right)^{6}\right] \tag{2}$$

where $\varepsilon_{ij} = (\varepsilon_i\varepsilon_j)^{1/2}$ and $R_{ij} = (R_i + R_j)/2$; R_i is the van der Waals radius; and ε_i is the characteristic energy for the Lennard-Jones potential. These expressions require three parameters for each atom type. For the atoms of nonzeolite molecules, standard CHARMM parameters[33] were used. However, for the atoms of the zeolite cluster, two sets of MM parameters were used, all of which are listed in Table 1. Parameter set P1 is that proposed by Zimmerman et al.,[15] and P2 is the new parameter set suggested in this work, for which optimization is described below.

Table 1. Charge and Lennard-Jones Parameters for O and Si Used in the QM/MM Portion of This Work

parameter set	Q_{Si}	Q_{O}	$\varepsilon_{\mathrm{Si}}$ (kcal/mol)	R_{Si} (Å)	ε_{O} (kcal/mol)	R_{O} (Å)
P1	0.7	−0.35	0.2	2.2	0.075	1.77
P2	0.7	−0.35	0.047	2.2	0.018	1.77

All the adsorption energies reported are ground-state electronic energies without zero-point vibrational corrections. The experimental electronic adsorption energies were derived by removing zero-point vibrational and temperature corrections from experimentally measured adsorption enthalpies

$$E_{\mathrm{ads}} = H_{\mathrm{ads}} - E_{\mathrm{cor}} \tag{3}$$

where E_{ads} is the adsorption energy; H_{ads} is the adsorption enthalpy; and E_{cor} is the sum of zero-point vibrational and temperature corrections. The correction term, E_{cor}, was calculated using a modified rigid rotor-harmonic oscillator approach (quasi-RRHO),[34] for which the vibrational energy contribution is described by

$$V = \sum_i V_i^{\text{quasi-RRHO}} = \sum_i \left[\omega(\nu_i) \times V_i^{\mathrm{RRHO}} + (1 - \omega(\nu_i)) \times \frac{1}{2}RT\right] \tag{4}$$

$$\omega(\nu_i) = \frac{1}{1 + (\nu_0/\nu_i)^4} \tag{5}$$

where T is the absolute temperature; R is the gas constant; ν_i is the frequency of the vibration mode i; ν_0 is chosen as 100 cm^{-1}; and V_i^{RRHO} is the vibrational energy contribution of mode i described by regular rigid rotor-harmonic approximation (RRHO)

$$V_i^{\mathrm{RRHO}} = \frac{1}{2}N_{\mathrm{A}}h\nu_i + RT\left(\frac{h\nu_i}{kT}\right)\frac{e^{-h\nu_i/kT}}{(1 - e^{-h\nu_i/kT})} \tag{6}$$

where N_{A} is the Avogadro constant; h is the Planck constant; and k is the Boltzmann constant. The rationale for using the quasi-RRHO instead of the RRHO is discussed below.

Geometry optimizations and single-point energy calculations were performed at the ωB97X-D/6-31G* and ωB97X-D/6-311++G(3df,3pd) levels of theory, respectively, unless noted otherwise. Frequency computations were performed on all structures to ensure that geometries corresponded to local minima or first-order saddle point (i.e., zero or one negative eigenvalues). All calculations were done using a development version of the Q-Chem software package.[35]

PARAMETER CALIBRATION

Since, as discussed previously, it is costly to do ab initio calculations of benchmark-level accuracy, experimental adsorption energies were taken as benchmarks in this work. Previous studies have indicated that the van der Waals interaction is the predominant interaction controlling physisorption of nonpolar molecules in zeolites, whereas the interactions of polar molecules or chemisorption in zeolites come from both van der Waals and electrostatic interactions.[15] Since there is no way to unravel interaction energies directly from experimental data, the adsorption energies of *n*-alkanes in siliceous MFI (silicalite), a prototypical physisorption case, were chosen to benchmark the Lennard-Jones parameters. In contrast to chemisorption at the active sites in zeolites, e.g., Brønsted or Lewis acid sites, there is no preferred binding site for dispersion-driven physisorption of *n*-alkanes in MFI.[36,37] However, as a first step toward studying the activation in H-MFI, we chose to investigate the adsorption of alkanes in the straight channel close to the T12 site, the site which is preferred for Al substitution.[22,23]

DOI: 10.1021/jp509921r
J. Phys. Chem. C 2015, 119, 1840−1850

The experimental values of adsorption enthalpies of C_1 to C_{10} *n*-alkanes in MFI,[38−47] noted as H_{ads}(expt), are shown in Figure 2. It is clear that even though there is a little uncertainty

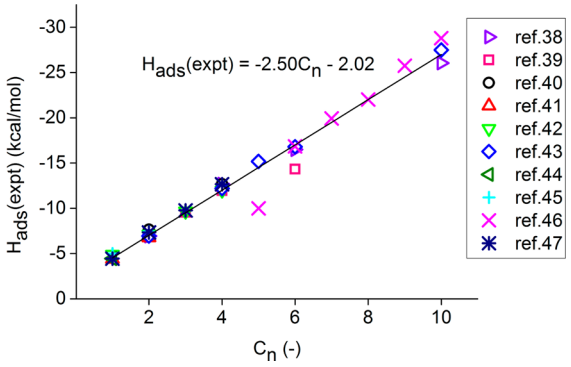

Figure 2. Adsorption enthalpies of linear alkanes in purely siliceous MFI as measured by experiments. C_n represents the number of carbon atoms in the alkane. The equation is the least-squares regression line of the data.

in the values reported by different authors, there is a good linear relationship between adsorption enthalpy and the number of carbon atoms in linear alkanes. The slope of the regression line, H'_{ads}(expt), reveals that the interaction energy between the zeolite and a CH_2 unit in an *n*-alkane is about −2.5 kcal/mol. The calculations carried out for the adsorption energies of methane to octane in the same zeolite using parameter set P1 are shown in Figure 3. The linear relationship

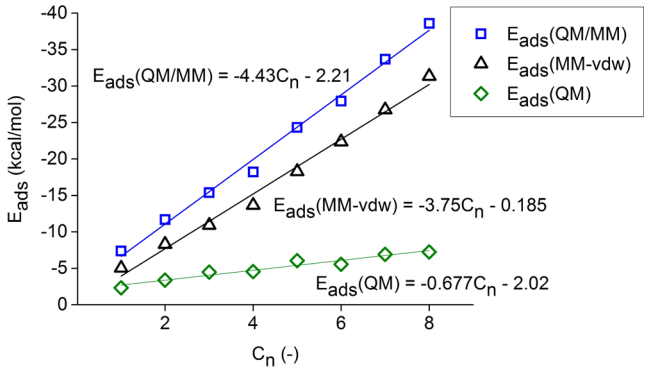

Figure 3. Adsorption energies of linear alkanes in MFI as calculated with QM/MM(P1). C_n represents the number of carbon atoms in the alkane. The equations are the least-squares regression lines of the data.

between the adsorption energy and the number of carbon atoms is reproduced, but with a slope of about −4.4 kcal/mol per CH_2 unit, which is much larger than the experimental result.

To get more insight into the interactions, we decomposed the calculated adsorption energies E_{ads}(QM/MM) into two components

$$E_{ads}(\text{QM/MM}) = E_{ads}(\text{MM−vdw}) + E_{ads}(\text{QM}) \quad (7)$$

where E_{ads}(MM−vdw) is the van der Waals interaction energy between an adsorbate and the atoms contained in the MM region, and E_{ads}(QM) is the sum of the QM−QM interaction energy between an adsorbate and the active site and the electrostatic interaction energy arising from the polarization of the adsorbate by the charges of the atoms contained in the MM region. The physical meanings of the slopes of the regression lines of E_{ads}(MM−vdw) and E_{ads}(QM), denoted as E'_{ads}(MM−vdw) and E'_{ads}(QM), are the adsorption energies per CH_2 unit arising from the two interactions, respectively. It is shown in Figure 3 that van der Waals interactions arising from the MM cluster, E'_{ads}(MM−vdw), are the dominant interaction, contributing about −3.8 kcal/mol per CH_2 unit, while E'_{ads}(QM) contributes only −0.7 kcal/mol. This finding agrees with the observation reported previously that physisorption of nonpolar molecules in zeolites is only sensitive to Lennard-Jones parameters[15] and clearly suggests that the characteristic energies of the Lennard-Jones potential ε_{Si} and ε_O in P1 are too large since E'_{ads}(MM−vdw) itself is larger than H'_{ads}(expt). What is not known, though, is whether the MM charge parameters also need to be revised since electrostatic interactions have only a minor effect on the adsorption of alkane in siliceous zeolites. However, we have shown previously that calculated intrinsic activation energies, which are sensitive to MM charge parameters, are in good agreement with experimental values;[18] therefore, we believe that the MM charge parameters assigned to Si and O of zeolite are reasonable.

Instead of reparameterizing the van der Waals parameters for Si and O de novo, a fine-tuning strategy was adopted. The correct MM van der Waals interaction per CH_2 unit with the cluster was calculated by subtracting E'_{ads}(QM) from H'_{ads}(expt). Then, a scaling factor for the P1 MM van der Waals interaction, *C*, was obtained as

$$C = (H'_{ads}(\text{expt}) - E'_{ads}(\text{QM}))/E'_{ads}(\text{MM−vdw}) \quad (8)$$

On the basis of the pairwise-additive nature of the Lennard-Jones potential energy, this scaling factor for the MM van der Waals interaction can be directly merged with ε_{Si} and ε_O in P1 keeping other parameters unchanged

$$C \times \varepsilon_{ij} = (C^2 \times \varepsilon_i \varepsilon_j)^{1/2} \quad (9)$$

$$\varepsilon_{Si}(\text{P2}) = C^2 \times \varepsilon_{Si}(\text{P1}) \quad (10)$$

$$\varepsilon_O(\text{P2}) = C^2 \times \varepsilon_O(\text{P1}) \quad (11)$$

where ε_i(X) is the characteristic energy of the Lennard-Jones potential of atom *i* in the parameter set X. The recalibrated parameter set, P2, is listed in Table 1.

The adsorption energies of C_1 to C_8 *n*-alkanes in siliceous MFI were calculated with QM/MM(P2) and were compared with experimental data and the values derived from QM/MM(P1). Figure 4a shows that QM/MM(P1) consistently overestimated the interactions, and the deviation increases with the size of the guest molecule. Since parameter set P1 was chosen to reproduce the results calculated at the ωB97X-D/6-31+G** level of theory, this parameter set inherited the basis set superposition error and the error that arises from ignoring many-body dispersion interactions, both of which contribute to overestimation of the interaction energy. Since the adsorbate−zeolite van der Waals interaction is modeled by the pairwise-additive Lennard-Jones potential in the QM/MM scheme, the error accumulates as the number of pairs of atoms between a guest molecule and a zeolite cluster increases, so the overbinding issue is inevitably more significant for larger guest molecules. On the other hand, Figure 4a shows that QM/MM with the recalibrated parameter set P2 accurately reproduces the experimental values.

DOI: 10.1021/jp509921r
J. Phys. Chem. C 2015, 119, 1840−1850

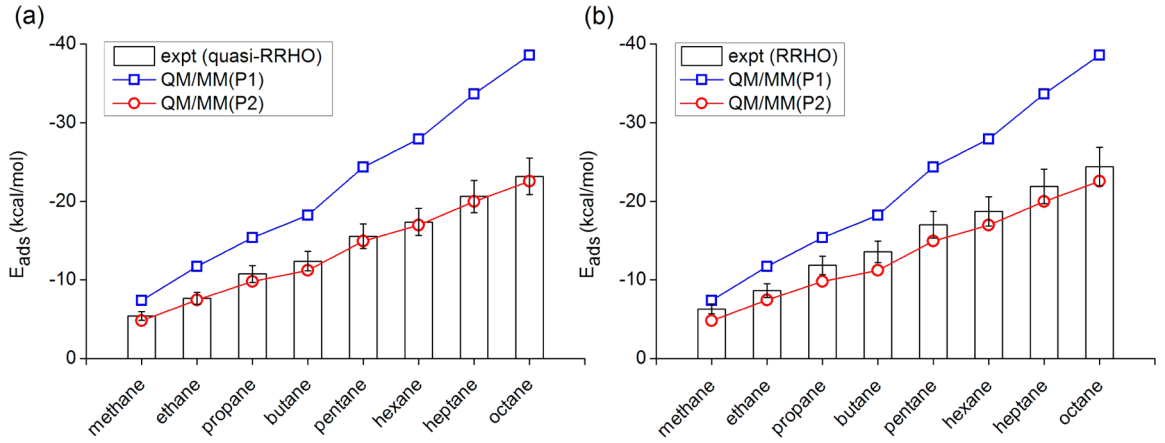

Figure 4. Adsorption energies of guest molecules in purely siliceous MFI calculated with QM/MM(P1) and QM/MM(P2). Experimental values[42,43,46] are shown with ±10% error bar and were derived by removing zero-point vibrational and temperature corrections from experimentally measured adsorption enthalpies using (a) quasi-RRHO and (b) RRHO. The connecting lines are drawn to guide the eye.

THERMAL CORRECTION

Because the scaling factor, C, was designed to fit the slope of the regression line of E_{ads}(QM/MM) in Figure 3 to H'_{ads}(expt), the underlying hypothesis of the recalibration is that E_{cor}, the sum of zero-point vibrational and temperature corrections, is not a function of the number of CH_2 units in linear alkanes. It turns out to be a good assumption since, as shown in Figure 4a, after removing E_{cor} calculated with the quasi-RRHO model from the experimental enthalpies the adsorption energies determined by QM/MM(P2) agree well with the experimental values. Interestingly, we found that if E_{cor} was determined by the RRHO model, though the slope of the experimental data can still be correctly reproduced by the calibrated parameters, QM/MM(P2) consistently underbinds by ∼2 kcal/mol comparing with the experimental data as shown in Figure 4b. As discussed previously, since the successful reproduction of the slope of the experimental adsorption energies of linear alkane adsorbed in siliceous zeolites indicates that the interaction between a CH_2 unit and the cluster in the MM region is correctly captured, it is not likely that the error comes from the MM parameters. Moreover, due to the fact that the offset is underbinding, it is not likely an error of using an incomplete basis set. On the other hand, it should not be cursorily attributed to density functional errors either because its magnitude is larger than the error expected for noncovalent interactions calculated with ωB97X-D.[16]

This finding motivates us to examine the energy contribution which is not directly determined by QM/MM(P2), i.e., the correction term E_{cor} calculated via the RRHO approximation. It is well-known that treating the translational and rotational modes of a guest molecule in a zeolite system as low-frequency vibrations via RRHO results in highly inaccurate entropy calculations.[48,49] However, to the best of our knowledge, the impact of this inaccurate treatment of modes on enthalpy calculations has not been discussed extensively. Using RRHO, the energy contributions of the translational and rotational modes are described by eq 6, the energy contribution of a harmonic oscillator. As $\nu_i \rightarrow 0$, eq 6 asymptotically approaches RT as opposed to $1/2RT$, the correct energy contribution of a translational or rotational mode, resulting in an error of $1/2\ RT$ per translational or rotational degree of freedom that a guest molecule retains in zeolites.

Since the error is proportional to temperature, one might expect it to be negligible if the temperature is not high. Unfortunately, we found that this issue could result in a noticeable error even at room temperature. This point can be elucidated by examining whether E_{cor} determined by RRHO lies between the upper and lower bounds defined by the extreme cases: mobile and immobile adsorptions. For the case of mobile adsorption, it is assumed that a guest molecule retains all of its translational and rotational modes in the zeolite. For the temperature range where the thermal excitation of vibrational modes is negligible ($T \leq 300$ K), E_{cor} for the mobile adsorption can be described as

$$E_{cor} = \Delta E_{ZPVE} - RT \tag{12}$$

where ΔE_{ZPVE} is the zero-point vibrational correction, and $-RT$ corresponds to the change of the PV term of the enthalpy for the adsorption of gas-phase molecules. On the other hand, for the case of immobile adsorption, it is assumed that a guest molecule loses all of its translational and rotational modes in the zeolite. Similarly, at low temperature, E_{cor} for the immobile adsorption case can be described as

$$E_{cor} = \Delta E_{ZPVE} - 4RT \tag{13}$$

The additional $-3RT$ corresponds to the loss of the translational and rotational energies in the immobile adsorption scenario.

Since the mobile and immobile cases are two extremes, for the range where the thermal excitation of vibrational modes is negligible ($T \leq 300$ K), eq 12 and eq 13 define the upper and lower bounds for E_{cor}. As shown in Figure 5, for the adsorption of methane in siliceous MFI, eq 12 and eq 13 define the allowed region (shaded area) in which E_{cor} should lie. However, Figure 5 clearly shows that E_{cor} determined by RRHO is within this region only if the temperature is very low ($T \leq 100$ K), and at room temperature ($T = 300$ K), the value determined by RRHO is about 1 kcal/mol higher than the upper bound. This issue is observed not only in the adsorption of methane but also in the adsorption of longer alkanes, such as n-octane adsorption in MFI (Figure 6). Since, as discussed previously, the error is proportional to temperature, it is critical to fix this artifact in order to accurately compute the adsorption or activation enthalpies above room temperature.

DOI: 10.1021/jp509921r
J. Phys. Chem. C 2015, 119, 1840−1850

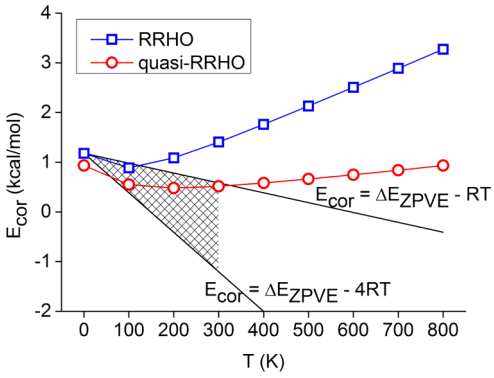

Figure 5. Sum of zero-point vibrational and temperature corrections, E_{cor}, determined by RRHO and quasi-RRHO for methane adsorption in purely siliceous MFI.

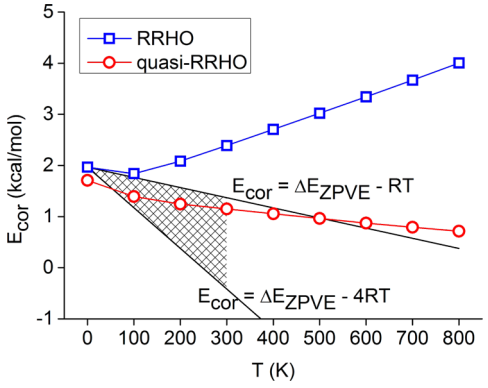

Figure 6. Sum of zero-point vibrational and temperature corrections, E_{cor}, determined by RRHO and quasi-RRHO for *n*-octane adsorption in purely siliceous MFI.

To remedy this problem, we replaced the energy contribution of the low-lying vibrational mode by $1/2RT$, the correct description for the energy of a translational or rotational mode, using the interpolation scheme described by eq 4. As shown in Figure 7, the quasi-RRHO scheme continuously interpolates between the harmonic vibrational and translational (or rotational) contributions using the Chai and Head-Gordon damping function[16] shown by eq 5 and effectively replaces the energy contribution for all modes with frequency less than ν_0 by $1/2RT$. Though this black-box type of interpolation procedure

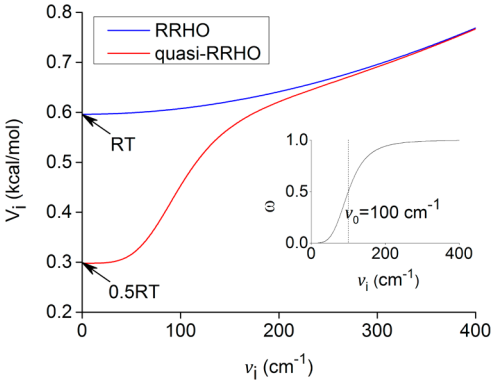

Figure 7. Energies of vibrational modes described by RRHO and quasi-RRHO models at 300 K. The cutoff frequency for the quasi-RRHO model, ν_0, is chosen as 100 cm^{-1}.

was originally proposed by Grimme to remedy the divergence issue of entropy calculation for low-lying modes of supramolecules,[34] we found that it is helpful to improve the accuracy of adsorption enthalpy calculations in zeolites. As shown in Figure 5, with the same cutoff frequency suggested by Grimme (100 cm^{-1}), it is clear that E_{cor} determined by quasi-RRHO behaves better than the one determined by RRHO for the adsorption of methane because it lies within the allowed region. The same improvement is observed in the case of the adsorption of longer alkanes, such as *n*-octane adsorption shown in Figure 6. Therefore, as shown in Figure 4a, the ~2 kcal/mol offset mentioned previously (Figure 4b) is not observed if E_{cor} is determined by the quasi-RRHO model.

One might have noticed from Figure 5 and Figure 6 that using the quasi-RRHO model also slightly affects ΔE_{ZPVE}, which is E_{cor} at 0 K. This is because, as shown by eq 4, the zero-point vibrational correction of mode *i*, $1/2N_A h\nu_i$, is also weighted by $\omega(\nu_i)$. This artifact can be avoided by using a slightly modified expression

$$V = \sum_i \left[\frac{1}{2} N_A h\nu_i + \omega(\nu_i) \times \left(RT \left(\frac{h\nu_i}{kT} \right) \frac{e^{-h\nu_i/kT}}{1 - e^{-h\nu_i/kT}} \right) + (1 - \omega(\nu_i)) \times \left(\frac{1}{2} RT \right) \right] \quad (14)$$

where $1/2N_A h\nu_i$ is factored out so that only the thermal excitation part of the vibrational contribution is weighted by $\omega(\nu_i)$. However, since the influence is small and the zero-point vibrational correction determined by RRHO is an approximation itself, we choose to adopt eq 4, the more physical expression which replaces all the energy contributed by a low-lying mode by $1/2RT$.

PARAMETER VALIDATION

To validate the parameter set, P2, the adsorption energies of two test sets were calculated with QM/MM(P2) and were compared with experimental data and the values derived from QM/MM(P1). The first test set covered the adsorption of nonane, decane, cyclohexane, 1-butene, and benzene in siliceous MFI. For this test set, dispersive interactions dominate the adsorbate−zeolite interactions so that the adsorption energy is only sensitive to Lennard-Jones parameters, as discussed above. Figure 8 shows that QM/MM(P2) outperforms QM/MM(P1) and correctly reproduces the experimental values for the entire test set, validating the superior ability of QM/MM(P2) to capture correctly dispersive interactions of adsorbates with zeolites.

The second test set examines the interactions of propane, NH_3, acetonitrile, 1-butene, pyridine, and methanol with H-MFI and CO_2, NH_3, and hexane with H-BEA. This test set covers polar molecules, which are more sensitive to long-range charge interactions with the lattice, and molecules that can strongly interact with the Brønsted acid site, i.e., NH_3 and pyridine. Figure 9 shows that QM/MM(P1) again overbinds all guest molecules. Pyridine, the largest polar guest molecule in the test set, deviates the most from the experimental value, consistent with the arguments given above. Without adjusting the MM charge parameters, parameter set P2 improved the accuracy of this test set, suggesting that the ε_{Si} and ε_O in P2 are compatible with the original MM charge parameters in P1. It also justifies the assumption that the charges assigned originally to Si and O atoms of the zeolite clusters in parameter set P1

DOI: 10.1021/jp509921r
J. Phys. Chem. C 2015, 119, 1840−1850

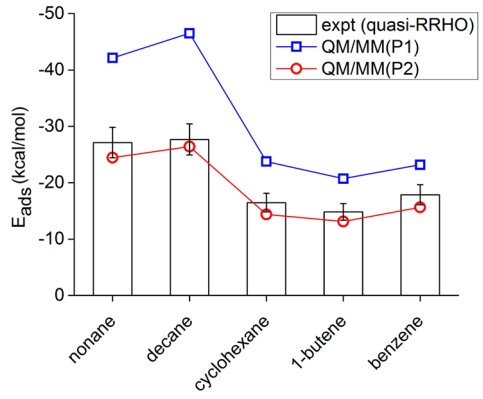

Figure 8. Adsorption energies of guest molecules in purely siliceous MFI calculated with QM/MM(P1) and QM/MM(P2). The experimental values of nonane,[46] decane,[43] cyclohexane,[60] 1-butene,[61] and benzene[62] are shown with ±10% error bar. The connecting lines are drawn to guide the eye.

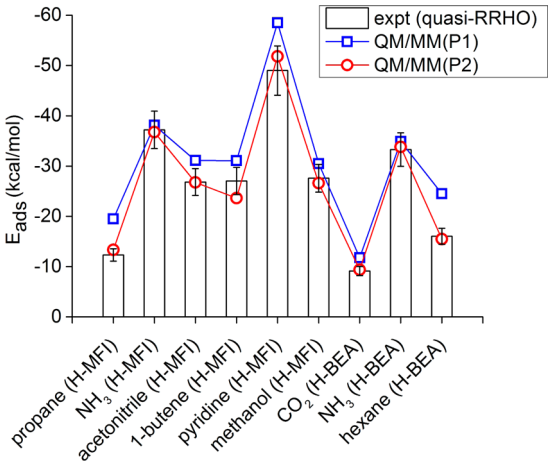

Figure 9. Adsorption energies of guest molecules in H-MFI and H-BEA calculated with QM/MM(P1) and QM/MM(P2). The experimental values of propane,[63] NH_3,[64] acetonitrile,[65] 1-butene,[66] pyridine,[64] and methanol[65] in H-MFI and CO_2,[67] NH_3,[68] and hexane[69] in H-BEA are shown with ±10% error bar. The connecting lines are drawn to guide the eye.

were reasonable and need not be modified. Moreover, the successful reproduction of the adsorption energies of CO_2, NH_3, and hexane in H-BEA observed experimentally using QM/MM(P2) suggests that though ε_{Si} and ε_O in parameter set P2 were trained to capture the dispersive interaction of alkane in MFI they are likely transferable to other zeolite systems.

The RMS error between the adsorption energies determined by QM/MM and observed experimentally were calculated for the test sets in MFI, H-MFI, and H-BEA to summarize the overall performance of QM/MM with parameter sets P1 and P2. As listed in Table 2, the RMS error is 8.3 kcal/mol using QM/MM(P1) at the ωB97X-D/6-311++G(3df,3pd) level of theory. By contrast, at the same level of theory, the RMS error is only 1.8 kcal/mol with P2, which validates the parameter set P2 for QM/MM calculations. An attempt was made to further reduce the RMS error by optimizing the scaling factor C using all the data sets as one single training set. Interestingly, the RMS error was only reduced by 0.1 kcal/mol via this procedure, which strongly supports the transferability of the recalibrated parameters.

Table 2. Statistical Errors of the Test Sets in MFI, H-MFI, and H-BEA[a]

parameter set	functional	basis set	MSE	MAE	RMS
P1	ωB97X-D	6-311++G(3df,3pd)	−6.7	6.7	8.3
P2	ωB97X-D	6-311++G(3df,3pd)	0.8	1.4	1.8
		Def2-TZVPD	0.8	1.6	1.9
P2	ωB97X-V	6-311++G(3df,3pd)	1.5	1.9	2.3
		Def2-TZVPD	1.6	1.9	2.4
P2	B97-D	6-311++G(3df,3pd)	1.0	1.7	2.0
		Def2-TZVPD	1.1	1.8	2.2
P2	M062X	6-311++G(3df,3pd)	2.5	2.6	3.0
		Def2-TZVPD	2.4	2.5	3.0
P2	B3LYP	6-311++G(3df,3pd)	6.5	6.5	7.2
		Def2-TZVPD	6.5	6.5	7.3

[a]Numbers are reported in kcal/mol.

Because the parameters were trained empirically with ωB97X-D/6-311++G(3df,3pd), we also examined the compatibility of P2 and other levels of theory (different basis sets or density functionals). As listed in Table 2, for all the functionals that we considered (ωB97X-D, ωB97X-V,[50] B97-D,[51] M062X,[52] and B3LYP[53,54]), the RMS error increases by less than 0.2 kcal/mol if 6-311++G(3df,3pd), the basis set used in the training process, is replaced by Def2-TZVPD. Since the 0.2 kcal/mol difference in RMS errors is small and the basis set 6-311++G(3df,3pd) only covers elements from H to Ar, we recommend using QM/MM(P2) with Def2-TZVPD, an effective core potential basis set covering elements from H to Rn, for systems containing elements heavier than Ar, e.g., Sn-BEA. As shown by the MSE listed in Table 2, QM/MM(P2) greatly underestimates the adsorption energies if B3LYP is used due to the absence of long-range dispersion interactions in the QM region.

On the other hand, though the accuracy of QM/MM(P2) is slightly degraded if ωB97X-V, B97-D, or M062X is used, the RMS errors calculated with ωB97X-V/6-311++G(3df,3pd) and B97-D/6-311++G(3df,3pd) (2.3 and 2.0 kcal/mol) are very close to the RMS error of ωB97X-D/6-311++G(3df,3pd) (1.8 kcal/mol), suggesting that although the parameter set P2 was trained with ωB97X-D it is compatible with ωB97X-V and B97-D. The compatibility of P2 and ωB97X-V is particularly important because the empirical long-range dispersion correction of ωB97X-D only supports period 1 to 5 elements, but there is great interest in studying reactivity of zeolites doped with elements of period 6, e.g., Hf and Pb.[30] It should be noted that though using QM/MM(P2) with B97-D performs almost as well as using QM/MM(P2) with ωB97X-D for the adsorption energies the use of B97-D is not recommended for calculating reaction barriers because it does take into account long-range exchange interactions. However, because of the low computational cost of using B97-D compared to ωB97X-D, we recommend using QM/MM(P2) with B97-D to explore reaction mechanisms and then using ωB97X-D for single-point energy computations in order to strike a balance between accuracy and computational cost. This point is illustrated by an example in the next section.

Though the above parametrization and validation were done for zeolite models containing a T5 QM cluster encompassing the active center, we found that the accuracy of QM/MM(P2) is not sensitive to the size of the QM cluster. For example, for the adsorption of pyridine in H-MFI, a case in which both the

DOI: 10.1021/jp509921r
J. Phys. Chem. C 2015, 119, 1840−1850

QM−QM and QM−MM interactions between the adsorbate and the zeolite are important, the adsorption energies calculated with T5 and T17 QM clusters (T5 QM/T432 MM and T17 QM/T420 MM) differ by only −0.18 kcal/mol at the ωB97X-D/6-311++G(3df,3pd) level of theory. Therefore, even though the parameters were designed for QM/MM calculations with a T5 QM cluster, one can use P2 with a QM region larger than T5 if needed, for purposes such as studying synergic effects of neighboring sites.[55,56] However, we note that if the QM region encompasses a significant part of the zeolite framework, in addition to dispersion-corrected DFT, an explicit correction might be needed for the nonadditive Axilrod−Teller−Muto three-body dispersion interaction, which increases with system size in order to obtain accurate dispersion interaction energies.[8]

GLUCOSE−FRUCTOSE ISOMERIZATION IN SN-BEA

The above discussion has focused on how the new parameter set P2 improves the performance of QM/MM calculations of adsorption energies. In this section, we illustrate how one can study a reaction occurring in zeolite efficiently and accurately using the P2 parameter set and the quasi-RRHO model. The P2 parameter set has been applied to study the isomerization of glucose to fructose in Sn-BEA and the synthesis of *p*-xylene from ethylene and 2,5-dimethylfuran in H-BEA.[30,57] The former is chosen as an example. The complete mechanism of this reaction and the details of the computations can be found in our recent work;[30] here we concentrate on the relative performance of parameter sets P1 and P2.

As shown in Scheme 1, glucose-to-fructose isomerization catalyzed by Sn-BEA is initiated by opening of the six-membered ring of glucopyranose to form acyclic glucose, which then undergoes isomerization to the acyclic form of fructose and subsequent ring closure to form fructofuranose.[29] The overall reaction rate is limited by a hydride shift from the C_2 carbon to the C_1 carbon, as shown by the transition state structure in Figure 10.[30] Starting with this structure, we calculated the apparent activation energy by redoing geometry optimizations and single-point calculations with the schemes listed in Table 3. Using ωB97X-D for both optimization (with the Def2-SV(P) basis) and single-point calculation (with the Def2-TZVPD basis), the apparent activation energy calculated with QM/MM(P1) is only 8.3 kcal/mol, which is much lower than the experimentally measured value of 21.2 kcal/mol.[29] As discussed above, this artifact is due to the overestimation of the van der Waals interaction between the zeolite and the reactant in the transition state so that it is impossible for QM/MM(P1) to reproduce experimental data even if the correct reaction mechanism is given unless the reactant is really small; i.e., the van der Waals interaction is negligible.

Scheme 1. Schematic Representation of the Isomerization of Glucopyranose to Fructofuranose[a]

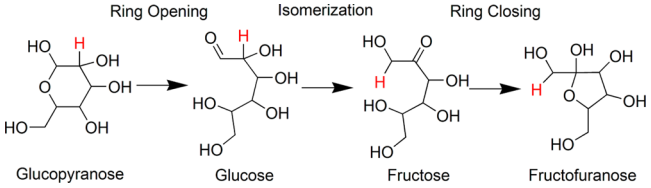

[a]The hydrogen atom marked as red is the one that undergoes a hydride shift.

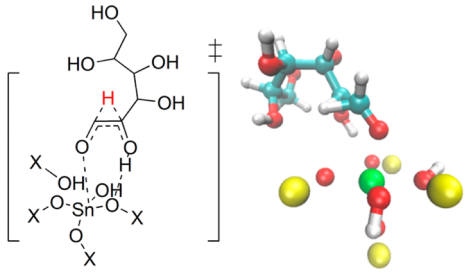

Figure 10. Rate-limiting transition state for glucose−fructose isomerization catalyzed by Sn-BEA.

Table 3. Apparent Activation Energy for Glucose−Fructose Isomerization Catalyzed by Sn-BEA at 343 K[a]

method	geometry optimization	single-point energy calculation	thermo correction	apparent activation energy (kcal/mol)
experiment	-	-	-	21.2 ± 0.7
QM/MM(P1)	ωB97X-D	ωB97X-D	RRHO	8.3
QM/MM(P2)	ωB97X-D	ωB97X-D	RRHO	22.3
QM/MM(P2)	ωB97X-D	ωB97X-D	quasi-RRHO	21.1
QM/MM(P2)	B97-D	ωB97X-D	quasi-RRHO	20.1

[a]The basis set used for geometry optimizations and single-point energy calculations are Def2-SV(P) and Def2-TZVPD, respectively.

On the other hand, using the same QM protocol, the apparent activation energy calculated with QM/MM(P2) and RRHO is 22.3 kcal/mol, which agrees well with the experimental value of 21.2 kcal/mol. The accuracy can be improved further if the thermal correction is calculated with the quasi-RRHO model. As listed in Table 3, the apparent activation energy calculated with QM/MM(P2) and quasi-RRHO is 21.1 kcal/mol, in excellent agreement with the experimental value. These results show that although the reparameterization of the QM/MM force fields is done using adsorption energies as training and test sets the new parameter set P2 greatly improves the accuracy of QM/MM calculations not only for adsorption energies but also for apparent activation energies. Bond-making and bond-breaking problems such as the isomerization transition state are the realm for which the QM/MM method was designed.

The good transferability of the parameter set P2 between the functionals (B97-D, ωB97X-D, and ωB97X-V) discussed in the previous section motivates us to pursue a more economical way of exploring mechanisms of complex reactions. Since the most expensive part of studying a reaction is identifying the correct reaction pathway, the computational cost can be greatly reduced if the potential energy surface walking procedures are carried out with a less computationally demanding but still sufficiently accurate functional. Indeed we already used the smaller Def2-SV(P) basis for geometry optimization and the larger Def2-TZVPD basis for single-point energies to reduce costs. Since advanced potential energy surface walking algorithms require only the first derivatives of the energy even for locating transition states,[58,59] we use the CPU time required to calculate first derivatives of the energy per step of

DOI: 10.1021/jp509921r
J. Phys. Chem. C 2015, 119, 1840−1850

the transition state search shown in Figure 10 as the index of computational costs.

As shown in Figure 11, because of the required six-dimensional numerical integral over the density and a nonlocal correlation kernel, ωB97X-V is more expensive than ωB97X-D so that there is no advantage in switching to ωB97X-V from the perspective of computational cost. On the other hand, B97-D is the lowest cost functional among those we examined, requiring only about one-third of the CPU time of ωB97X-D. This result suggests that the costs of the potential energy surface walking procedures can be roughly reduced by a factor of 3 with little or no degradation of the accuracy if the geometry optimized with B97-D is close to that of ωB97X-D.

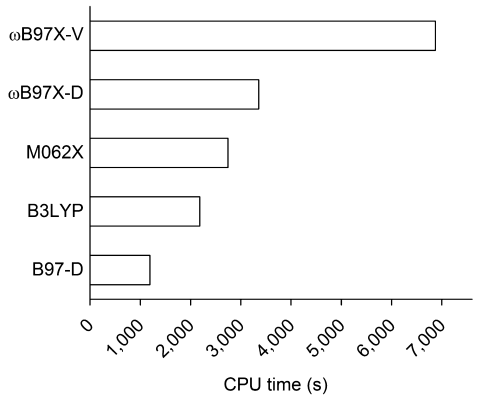

Figure 11. CPU time required to calculate first derivatives of the energy of the transition state shown in Figure 10. The basis set used for the calculations is Def2-SV(P). All timings were performed using a development version of the software package Q-Chem on a single core of a dual 2.4 GHz AMD Istanbul 6-core processor machine allotted 48 GB of RAM.

As listed in Table 3, the scheme using B97-D for geometry optimizations and ωB97X-D for single-point energy calculations works well, since the calculated apparent activation energy (20.1 kcal/mol) is close to the experimental value (21.2 ± 0.7 kcal/mol) and deviates by only 1 kcal/mol from the result of the scheme using ωB97X-D for all the calculations (21.1 kcal/mol). Since the small difference between the geometries optimized with B97-D and ωB97X-D can always be removed with little effort by performing a geometry optimization using ωB97X-D starting with the B97-D optimized geometry, an optimization procedure which should converge rapidly in a few steps, it is highly recommended that QM/MM(P2) with B97-D be used to explore the reaction mechanism of a complex reaction in order to reduce computational cost.

■ DISCUSSION AND CONCLUSIONS

Electrostatically embedded QM/MM simulations are computationally appealing methods for performing zeolite simulations, although the accuracy is highly dependent on the MM parameters. A previously reported parameter set (P1), chosen to minimize the RMS deviations of adsorption energies compared with full QM ωB97X-D/6-31+G** adsorption energies in small clusters, is shown to lead to systematic overbinding of adsorbate molecules in zeolites, with errors increasing with adsorbate size. Consistent with this finding, QM/MM(P1) overbinds C_1 to C_8 *n*-alkanes in siliceous MFI where the dispersive interaction dominates the adsorption energies. To address this issue, a new parameter set P2 (see Table 1) is optimized by directly scaling the characteristic energies of the Lennard-Jones potential of O and Si in P1. The scaling factor was chosen to modify the QM/MM(P1) MM van der Waals interactions so that the calculated alkane adsorption energies agree with those measured experimentally.

Adsorption energies determined from QM/MM(P2) agree to within a RMS deviation of 1.8 kcal/mol with experimental values for two test sets, which cover both physisorption and chemisorption of guest molecules in MFI, H-MFI, and H-BEA. By contrast, the RMS deviation for QM/MM(P1) is 8.3 kcal/mol for the same test sets. This small RMS error compared with experimental values and the significant improvement relative to QM/MM(P1) validate the ability of QM/MM(P2) to better capture correctly dispersive interactions of adsorbates with zeolites. Though the parameter set P2 is trained empirically at the ωB97X-D/6-311++G(3df,3pd) level of theory, it is shown to be compatible with the basis set Def2-TZVPD and the functionals B97-D and ωB97X-V because the RMS error varies by less than 0.6 kcal/mol between these levels of theory.

The accuracy of thermal correction for adsorption enthalpies determined by the rigid rotor-harmonic oscillator approximation (RRHO) is examined by comparing with the values derived based on mobile and immobile adsorption assumptions (Figure 5 and Figure 6). It is shown by the adsorption of *n*-alkane in MFI that the values determined by RRHO are overestimated even if the temperature is not high (≲300 K). The error is attributed to treating the translational and rotational degrees of freedom retained by guest molecules in zeolites as low frequency vibrational modes. The deviation is remedied by using a modified quasi-RRHO scheme, which effectively replaces the energy contribution of low-lying vibrational modes with the energy of free translational and rotational modes. While quasi-RRHO methods have been previously used to correct entropies of adsorption, the need to correct RRHO contributions to enthalpies has not previously been discussed.

Glucose-to-fructose isomerization catalyzed by Sn-BEA is taken as an example to demonstrate the transferability of the new parameter set P2 and the usefulness of the quasi-RRHO model in the calculations of apparent activation energies. Using QM/MM(P1) and RRHO, the calculated apparent activation energy is 8.3 kcal/mol, which deviates significantly from the experimentally observed value of 21.2 kcal/mol. By contrast, at the same level of theory, the activation energies calculated using QM/MM(P2) with RRHO and quasi-RRHO are 22.3 and 21.1 kcal/mol, respectively, in very good agreement with the experimental value. Though this high accuracy was achieved by treating the QM region with ωB97X-D for both geometry optimizations and single-point energy calculations, we found that the same level of accuracy can be achieved using B97-D for geometry optimization and ωB97X-D for single-point energy calculation with roughly only one-third of the original costs. Therefore, it is recommended that QM/MM(P2) with B97-D be used to explore reaction pathways for complex systems in order to reduce computational costs.

Turning to ongoing work, the good transferability of the parameters in the cases reported here motivates us to explore the possibility of applying them to chemistry in zeolites which are neither siliceous nor in their Brønsted acid form. One useful extension is the application to cation-containing frameworks such as Na−X zeolite. The supercage structure of Na−X imparts a lower framework density and hence fewer adsorbate−

DOI: 10.1021/jp509921r
J. Phys. Chem. C 2015, 119, 1840−1850

framework interactions. Interestingly, though cation-containing frameworks are not the systems for which our P2 parameters were originally optimized, QM/MM(P2) reproduces experimental adsorption energies for C_1−C_7 alkanes after modification of the charge scheme to include Q_{Na} = +1.0. This work is forthcoming as part of a study to determine the optimal QM/MM charge parameters for low Si/Al ratio zeolites.

AUTHOR INFORMATION

Corresponding Author

*E-mail: mhg@cchem.berkeley.edu.

Notes

The authors declare no competing financial interest.

ACKNOWLEDGMENTS

This work was supported by the XC^2 program funded by BP, with additional support through the National Science Foundation (Grant CHE-1265731).

REFERENCES

(1) Corma, A. Inorganic Solid Acids and Their Use in Acid-Catalyzed Hydrocarbon Reactions. *Chem. Rev.* **1995**, *95*, 559−614.

(2) Vermeiren, W.; Gilson, J.-P. Impact of Zeolites on the Petroleum and Petrochemical Industry. *Top. Catal.* **2009**, *52*, 1131−1161.

(3) Moliner, M.; Román-Leshkov, Y.; Davis, M. E. Tin-Containing Zeolites Are Highly Active Catalysts for the Isomerization of Glucose in Water. *Proc. Natl. Acad. Sci. U.S.A.* **2010**, *107*, 6164−6168.

(4) Yu, J.; Xu, R. Rational Approaches toward the Design and Synthesis of Zeolitic Inorganic Open-Framework Materials. *Acc. Chem. Res.* **2010**, *43*, 1195−1204.

(5) Janda, A.; Bell, A. T. Effects of Si/Al Ratio on the Distribution of Framework Al and on the Rates of Alkane Monomolecular Cracking and Dehydrogenation in H-MFI. *J. Am. Chem. Soc.* **2013**, *135*, 19193−19207.

(6) Bell, A. T.; Head-Gordon, M. Quantum Mechanical Modeling of Catalytic Processes. *Annu. Rev. Chem. Biomol. Eng.* **2011**, *2*, 453−477.

(7) Klimeš, J.; Michaelides, A. Perspective: Advances and Challenges in Treating van Der Waals Dispersion Forces in Density Functional Theory. *J. Chem. Phys.* **2012**, *137*, 120901−120912.

(8) Risthaus, T.; Grimme, S. Benchmarking of London Dispersion-Accounting Density Functional Theory Methods on Very Large Molecular Complexes. *J. Chem. Theory Comput.* **2013**, *9*, 1580−1591.

(9) Gomes, J.; Zimmerman, P. M.; Head-Gordon, M.; Bell, A. T. Accurate Prediction of Hydrocarbon Interactions with Zeolites Utilizing Improved Exchange-Correlation Functionals and QM/MM Methods: Benchmark Calculations of Adsorption Enthalpies and Application to Ethene Methylation by Methanol. *J. Phys. Chem. C* **2012**, *116*, 15406−15414.

(10) Lin, H.; Truhlar, D. G. QM/MM: What Have We Learned, Where Are We, and Where Do We Go from Here? *Theor. Chem. Acc.* **2007**, *117*, 185−199.

(11) Bakowies, D.; Thiel, W. Hybrid Models for Combined Quantum Mechanical and Molecular Mechanical Approaches. *J. Phys. Chem.* **1996**, *100*, 10580−10594.

(12) Clark, L. A.; Sierka, M.; Sauer, J. Computational Elucidation of the Transition State Shape Selectivity Phenomenon. *J. Am. Chem. Soc.* **2004**, *126*, 936−947.

(13) Lomratsiri, J.; Probst, M.; Limtrakul, J. Structure and Adsorption of a Basic Probe Molecule on H-ZSM-5 Nanostructured Zeolite: An Embedded ONIOM Study. *J. Mol. Graph. Model.* **2006**, *25*, 219−225.

(14) Shor, A. M.; Shor, E. A. I.; Laletina, S.; Nasluzov, V. A.; Vayssilov, G. N.; Roesch, N. Effect of the Size of the Quantum Region in a Hybrid Embedded-Cluster Scheme for Zeolite Systems. *Chem. Phys.* **2009**, *363*, 33−41.

(15) Zimmerman, P. M.; Head-Gordon, M.; Bell, A. T. Selection and Validation of Charge and Lennard-Jones Parameters for QM/MM Simulations of Hydrocarbon Interactions with Zeolites. *J. Chem. Theory Comput.* **2011**, *7*, 1695−1703.

(16) Chai, J.-D.; Head-Gordon, M. Long-Range Corrected Hybrid Density Functionals with Damped Atom−atom Dispersion Corrections. *Phys. Chem. Chem. Phys.* **2008**, *10*, 6615−6620.

(17) Chai, J.-D.; Head-Gordon, M. Systematic Optimization of Long-Range Corrected Hybrid Density Functionals. *J. Chem. Phys.* **2008**, *128*, 084106−084115.

(18) Sharada, S. M.; Zimmerman, P. M.; Bell, A. T.; Head-Gordon, M. Insights into the Kinetics of Cracking and Dehydrogenation Reactions of Light Alkanes in H-MFI. *J. Phys. Chem. C* **2013**, *117*, 12600−12611.

(19) Olson, D. H.; Kokotailo, G. T.; Lawton, S. L.; Meier, W. M. Crystal Structure and Structure-Related Properties of ZSM-5. *J. Phys. Chem.* **1981**, *85*, 2238−2243.

(20) Newsam, J. M.; Treacy, M. M. J.; Koetsier, W. T.; Gruyter, C. B. D. Structural Characterization of Zeolite Beta. *Proc. R. Soc. London Ser. Math. Phys. Sci.* **1988**, *420*, 375−405.

(21) Olson, D. H. Reinvestigation of the Crystal Structure of the Zeolite Hydrated NaX. *J. Phys. Chem.* **1970**, *74*, 2758−2764.

(22) Olson, D. H.; Khosrovani, N.; Peters, A. W.; Toby, B. H. Crystal Structure of Dehydrated CsZSM-5 (5.8A1): Evidence for Nonrandom Aluminum Distribution. *J. Phys. Chem. B* **2000**, *104*, 4844−4848.

(23) Mentzen, B. F.; Sacerdote-peronnet, M. Prediction of Preferred Proton Locations in HMFI/benzene Complexes by Molecular Mechanics Calculations. Comparison with Nmr, Structural and Calorimetric Results. *Mater. Res. Bull.* **1994**, *29*, 1341−1348.

(24) Xiu-Liang, S.; Chong-Pin, H.; Jie, Z.; Biao-Hua, C. Location of Al and Acid Strength of Bronsted Acid in Beta Zeolite. *Acta Phys.-Chim. Sin.* **2009**, *25*, 1136−1142.

(25) Bare, S. R.; Kelly, S. D.; Sinkler, W.; Low, J. J.; Modica, F. S.; Valencia, S.; Corma, A.; Nemeth, L. T. Uniform Catalytic Site in Sn-B-Zeolite Determined Using X-Ray Absorption Fine Structure. *J. Am. Chem. Soc.* **2005**, *127*, 12924−12932.

(26) Shetty, S.; Pal, S.; Kanhere, D.; Goursot, A. Structural, Electronic, and Bonding Properties of Zeolite Sn-Beta: A Periodic Density Functional Theory Study RID C-5835−2009. *Chem.−Eur. J.* **2005**, *12*, 518−523.

(27) Boronat, M.; Concepción, P.; Corma, A.; Renz, M.; Valencia, S. Determination of the Catalytically Active Oxidation Lewis Acid Sites in Sn-Beta Zeolites, and Their Optimisation by the Combination of Theoretical and Experimental Studies. *J. Catal.* **2005**, *234*, 111−118.

(28) Boronat, M.; Corma, A.; Renz, M. Mechanism of the Meerwein-Ponndorf-Verley-Oppenauer (MPVO) Redox Equilibrium on Sn- and Zr-Beta Zeolite Catalysts RID B-9361−2011. *J. Phys. Chem. B* **2006**, *110*, 21168−21174.

(29) Bermejo-Deval, R.; Assary, R. S.; Nikolla, E.; Moliner, M.; Román-Leshkov, Y.; Hwang, S.-J.; Palsdottir, A.; Silverman, D.; Lobo, R. F.; Curtiss, L. A.; et al. Metalloenzyme-like Catalyzed Isomerizations of Sugars by Lewis Acid Zeolites. *Proc. Natl. Acad. Sci. U.S.A.* **2012**, *109*, 9727−9732.

(30) Li, Y.-P.; Head-Gordon, M.; Bell, A. T. Analysis of the Reaction Mechanism and Catalytic Activity of Metal-Substituted Beta Zeolite for the Isomerization of Glucose to Fructose. *ACS Catal.* **2014**, *4*, 1537−1545.

(31) Foloppe, N.; MacKerell, A. D., Jr. All-Atom Empirical Force Field for Nucleic Acids: I. Parameter Optimization Based on Small Molecule and Condensed Phase Macromolecular Target Data. *J. Comput. Chem.* **2000**, *21*, 86−104.

(32) Yin, D.; MacKerell, A. D. Combined Ab Initio/empirical Approach for Optimization of Lennard−Jones Parameters. *J. Comput. Chem.* **1998**, *19*, 334−348.

(33) Vanommeslaeghe, K.; Hatcher, E.; Acharya, C.; Kundu, S.; Zhong, S.; Shim, J.; Darian, E.; Guvench, O.; Lopes, P.; Vorobyov, I.; et al. CHARMM General Force Field: A Force Field for Drug-like Molecules Compatible with the CHARMM All-Atom Additive Biological Force Fields. *J. Comput. Chem.* **2010**, *31*, 671−690.

DOI: 10.1021/jp509921r
J. Phys. Chem. C 2015, 119, 1840−1850

(34) Grimme, S. Supramolecular Binding Thermodynamics by Dispersion-Corrected Density Functional Theory. *Chem.—Eur. J.* **2012**, *18*, 9955−9964.
(35) Shao, Y.; Gan, Z.; Epifanovsky, E.; Gilbert, A. T. B.; Wormit, M.; Kussmann, J.; Lange, A. W.; Behn, A.; Deng, J.; Feng, X.; et al. Advances in Molecular Quantum Chemistry Contained in the Q-Chem 4 Program Package. *Mol. Phys.* **2015**, *113*, 184−215.
(36) Smit, B.; Siepmann, J. I. Computer Simulations of the Energetics and Siting of N-Alkanes in Zeolites. *J. Phys. Chem.* **1994**, *98*, 8442−8452.
(37) Smit, B.; Siepmann, J. I. Simulating the Adsorption of Alkanes in Zeolites. *Science* **1994**, *264*, 1118−1120.
(38) Stach, H.; Lohse, U.; Thamm, H.; Schirmer, W. Adsorption Equilibria of Hydrocarbons on Highly Dealuminated Zeolites. *Zeolites* **1986**, *6*, 74−90.
(39) Richards, R.; Rees, L. Sorption and Packing of Normal-Alkane Molecules in Zsm-5. *Langmuir* **1987**, *3*, 335−340.
(40) Thamm, H. Adsorption Site Heterogeneity in Silicalite: A Calorimetric Study. *Zeolites* **1987**, *7*, 341−346.
(41) Choudhary, V. R.; Mayadevi, S. Adsorption of Methane, Ethane, Ethylene, and Carbon Dioxide on High Silica Pentasil Zeolites and Zeolite-like Materials Using Gas Chromatography Pulse Technique. *Sep. Sci. Technol.* **1993**, *28*, 2197−2209.
(42) Hufton, J. R.; Danner, R. P. Chromatographic Study of Alkanes in Silicalite: Equilibrium Properties. *AIChE J.* **1993**, *39*, 954−961.
(43) Stach, H.; Fiedler, K.; Janchen, J. Correlation between Initial Heats of Adsorption and Structural Parameters of Molecular Sieves with Different Chemical Composition - a Calorimetric Study. *Pure Appl. Chem.* **1993**, *65*, 2193−2200.
(44) Golden, T. C.; Sircar, S. Gas Adsorption on Silicalite. *J. Colloid Interface Sci.* **1994**, *162*, 182−188.
(45) Dunne, J. A.; Rao, M.; Sircar, S.; Gorte, R. J.; Myers, A. L. Calorimetric Heats of Adsorption and Adsorption Isotherms. 2. O2, N2, Ar, CO2, CH4, C2H6, and SF6 on NaX, H-ZSM-5, and Na-ZSM-5 Zeolites. *Langmuir* **1996**, *12*, 5896−5904.
(46) Sun, M. S.; Talu, O.; Shah, D. B. Adsorption Equilibria of C-5-C-10 Normal Alkanes in Silicalite Crystals. *J. Phys. Chem.* **1996**, *100*, 17276−17280.
(47) Zhu, W.; van de Graaf, J. M.; van den Broeke, L. J. P.; Kapteijn, F.; Moulijn, J. A. TEOM: A Unique Technique for Measuring Adsorption Properties. Light Alkanes in Silicalite-1. *Ind. Eng. Chem. Res.* **1998**, *37*, 1934−1942.
(48) De Moor, B. A.; Reyniers, M.-F.; Marin, G. B. Physisorption and Chemisorption of Alkanes and Alkenes in H-FAU: A Combined Ab Initio−statistical Thermodynamics Study. *Phys. Chem. Chem. Phys.* **2009**, *11*, 2939−2958.
(49) De Moor, B. A.; Reyniers, M.-F.; Gobin, O. C.; Lercher, J. A.; Marin, G. B. Adsorption of C2-C8 N-Alkanes in Zeolites. *J. Phys. Chem. C* **2011**, *115*, 1204−1219.
(50) Mardirossian, N.; Head-Gordon, M. ωB97X-V: A 10-Parameter, Range-Separated Hybrid, Generalized Gradient Approximation Density Functional with Nonlocal Correlation, Designed by a Survival-of-the-Fittest Strategy. *Phys. Chem. Chem. Phys.* **2014**, *16*, 9904−9924.
(51) Grimme, S. Semiempirical GGA-Type Density Functional Constructed with a Long-Range Dispersion Correction. *J. Comput. Chem.* **2006**, *27*, 1787−1799.
(52) Zhao, Y.; Truhlar, D. G. The M06 Suite of Density Functionals for Main Group Thermochemistry, Thermochemical Kinetics, Noncovalent Interactions, Excited States, and Transition Elements: Two New Functionals and Systematic Testing of Four M06-Class Functionals and 12 Other Functionals. *Theor. Chem. Acc.* **2008**, *120*, 215−241.
(53) Becke, A. D. Density-Functional Exchange-Energy Approximation with Correct Asymptotic Behavior. *Phys. Rev. A* **1988**, *38*, 3098−3100.
(54) Lee, C.; Yang, W.; Parr, R. Development of the Colle-Salvetti Correlation-Energy Formula into a Functional of the Electron-Density. *Phys. Rev. B* **1988**, *37*, 785−789.
(55) Yang, G.; Pidko, E. A.; Hensen, E. J. M. Structure, Stability, and Lewis Acidity of Mono and Double Ti, Zr, and Sn Framework Substitutions in BEA Zeolites: A Periodic Density Functional Theory Study. *J. Phys. Chem. C* **2013**, *117*, 3976−3986.
(56) Hanna, D. G.; Shylesh, S.; Li, Y.-P.; Krishna, S.; Head-Gordon, M.; Bell, A. T. Experimental and Theoretical Study of N-Butanal Self-Condensation over Ti Species Supported on Silica. *ACS Catal.* **2014**, *4*, 2908−2916.
(57) Li, Y.-P.; Head-Gordon, M.; Bell, A. T. Computational Study of P-Xylene Synthesis from Ethylene and 2,5-Dimethylfuran Catalyzed by H-BEA. *J. Phys. Chem. C* **2014**, *118*, 22090−22095.
(58) Sharada, S. M.; Zimmerman, P. M.; Bell, A. T.; Head-Gordon, M. Automated Transition State Searches without Evaluating the Hessian. *J. Chem. Theory Comput.* **2012**, *8*, 5166−5174.
(59) Sharada, S. M.; Bell, A. T.; Head-Gordon, M. A Finite Difference Davidson Procedure to Sidestep Full Ab Initio Hessian Calculation: Application to Characterization of Stationary Points and Transition State Searches. *J. Chem. Phys.* **2014**, *140*, 164115.
(60) Cavalcante, C.; Ruthven, D. Adsorption of Branched and Cyclic Paraffins in Silicalite. 1. Equilibrium. *Ind. Eng. Chem. Res.* **1995**, *34*, 177−184.
(61) Thamm, H.; Stach, H.; Fiebig, W. Calorimetric Study of the Absorption of N-Butane and but-L-Ene on a Highly Dealuminated Y-Type Zeolite and on Silicalite. *Zeolites* **1983**, *3*, 95−97.
(62) Thamm, H. Calorimetric Study on the State of Aromatic Molecules Sorbed on Silicalite. *J. Phys. Chem.* **1987**, *91*, 8−11.
(63) Eder, F.; Stockenhuber, M.; Lercher, J. A. Bronsted Acid Site and Pore Controlled Siting of Alkane Sorption in Acidic Molecular Sieves. *J. Phys. Chem. B* **1997**, *101*, 5414−5419.
(64) Parrillo, D.; Lee, C.; Gorte, R. Heats of Adsorption for Ammonia and Pyridine in H-Zsm-5 - Evidence for Identical Bronsted-Acid Sites. *Appl. Catal.-Gen.* **1994**, *110*, 67−74.
(65) Lee, C. C.; Gorte, R. J.; Farneth, W. E. Calorimetric Study of Alcohol and Nitrile Adsorption Complexes in H-ZSM-5. *J. Phys. Chem. B* **1997**, *101*, 3811−3817.
(66) Lechert, H.; Schweitzer, W. Gas Chromatographic Sorption Studies of Hydrocarbons in Pentasils with Different Si/Al-Ratio. *Proc. 6th Int. Zeolite Conf.* **1983**, 210.
(67) Rodriguez Delgado, M.; Otero Arean, C. Carbon Monoxide, Dinitrogen and Carbon Dioxide Adsorption on Zeolite H-Beta: IR Spectroscopic and Thermodynamic Studies. *Energy* **2011**, *36*, 5286−5291.
(68) Suzuki, K.; Sastre, G.; Katada, N.; Niwa, M. Quantitative Measurements of Brønsted Acidity of Zeolites by Ammonia IRMS−TPD Method and Density Functional Calculation. *Chem. Lett.* **2007**, *36*, 1034−1035.
(69) Kotrel, S.; Rosynek, M. P.; Lunsford, J. H. Intrinsic Catalytic Cracking Activity of Hexane over H-ZSM-5, H-β and H-Y Zeolites. *J. Phys. Chem. B* **1999**, *103*, 818−824.

DOI: 10.1021/jp509921r
J. Phys. Chem. C 2015, 119, 1840−1850